Journal of Asian Concrete Federation

journal homepage: https://jacf.sfulib3.publicknowledgeproject.org/index.php/jacf

The Coupled Influence of Size and Strain Rate on the Failure Mechanism and Model Prediction of Fly Ash Concrete

Yaojie Lian*

National Key Laboratory of Intelligent Construction and Operation and Maintenance of Water Resources Engineering, Tianjin University, Tianjin 300000, China

A B S T R A C T

This study investigates the mechanical behavior and failure characteristics of fly ash concrete under quasi-static to low-to-medium strain rate loading. Uniaxial compression tests were conducted on three specimen sizes under four strain rate conditions (totaling 12 working conditions), analyzing damage evolution and failure patterns across different scales and loading rates. Results indicate that at lower strain rates, uniformly distributed cracks formed on specimen surfaces, with damage concentrated at coarse aggregate-mortar interfaces. In contrast, higher strain rates induced brittle failure characterized by crack propagation along the loading direction and coarse aggregate fracture - particularly evident in smaller specimens. As strain rates increased, the compressive strength of small, medium, and large specimens rose by 48.18%, 38.19%, and 29.07% respectively, demonstrating diminishing strength enhancement and reduced strain rate sensitivity with larger dimensions. Based on Weibull and log-normal statistical models, this study introduces a coupling coefficient accounting for size and strain rate effects, establishing a novel dynamic strength model capable of predicting stress-strain responses within target strain rate ranges. The model provides theoretical support for optimizing fly Ash cement-based materials and offers valuable references for durability assessment in hydraulic and civil engineering structures.

Keywords: Fly ash concrete; Size effect; Strain rate effect; Experimental study; Statistical distribution model; Eco-friendly concrete

Introduction

Fly ash concrete has become a key material widely used in hydraulic engineering due to its environmentally friendly nature, high density, high durability, strong resistance to erosion and abrasion, and excellent impermeability [1, 2]. With the continuous development of design theories for fly Ash cement-based materials, there is a growing need to systematically reveal the macroscopic mechanical response mechanisms of such materials. The nonlinear mechanical behavior of concrete is influenced not only by the characteristics and spatial distribution of its components but also significantly by structural size and shape. This is particularly evident in hydraulic infrastructure dominated by large-volume components, making in-depth study of the size effect essential for achieving fly Ash material design and performance control. On the other hand, fly Ash cement-based materials must possess the ability to respond fly Ash to dynamic loads (e.g., earthquakes and impacts) in real service environments. The notable strain rate effect exhibited by concrete is directly related to its damage evolution and failure modes under dynamic conditions, serving as an important basis for evaluating the material's self-sensing and impact-resistant functionalities. As engineering structures evolve toward intelligence and high performance, systematic research on the size effect of fly ash concrete under quasi-static to low-to-medium strain rate loading will not only enhance the understanding of its dynamic mechanical behavior across multiple scales but also provide theoretical foundations and data support for the modeling, lifespan prediction, and

* Corresponding author: Yaojie Lian (lianyaojie@126.com)

DOI http://dx.doi.org/10.18702/acf.2026.12.3.1

Received: 19-Jan-2026; Revised: 14-May-2026; Accepted: 11-Jun-2026; Published online: 31-Jul-2026

ISSN 2465-7964, eISSN 2465-7972. Copyright © Asian Concrete Federation, All rights reserved.

sustainable maintenance of such materials in future fly Ash hydraulic infrastructure [3].

As a complex subject in material science, concrete size effect is closely related to the aggregate distribution, aggregate particle size, concrete porosity and strength grade. In the existing literature, the size effect is usually examined by scientific experiment, theoretical modeling and/or numerical analysis [4-11]. For example, Lee et al. [5] carried out static and dynamic compression tests on 120 concrete cylinders by considering the strength grades of 30MPa, 35MPa and 40MPa, and the dimensions of 150×300mm and 100×200mm. Their results showed that concrete with a higher strength grade would exhibit a more obvious size effect on its compressive strength. Chen et al. [6] performed compression tests on 24 concrete cylinders with the diameter ranged from 150mm to 460mm and the strength grade of C60 and C45, and reported that the axial compressive strength and peak strain of concrete were negatively correlated with the sample size. To date, the mechanism of size effect has been explained by many researchers from different perspectives. For instance, Bazant [12, 13] proposed the fracture mechanics size effect theory based on energy release; Weibull [14] proposed the statistical size effect theory based on the "weakest chain" concept; and Carpinteri [15] proposed the size effect theory by considering the influence of crack fractal characteristics on the tensile strength and fracture energy of concrete-like materials. Wu et al. [16] investigated the influence of fly ash with different particle sizes on the performance of mortar. The results showed that fly ash with a particle size range of 10–20 μm resulted in the lowest total porosity (12.88%), the smallest average pore diameter (27.1 nm), and the smallest most probable pore diameter (21.2 nm) in the cement mortar. This led to a reduction in harmful pores and an increase in harmless pores, resulting in a denser microstructure and improved durability. Although the type of hydration products remained unchanged across different fly ash particle sizes, a smaller particle size led to a more complete pozzolanic reaction, thereby exerting a more pronounced promoting effect on the hydration of the mortar.

Following the change of strain rate, the mechanical behaviors and properties of a material may also change to varying degrees. This phenomenon is known as the strain rate effect, and concrete is a typical composite material with a significant strain rate effect. The mechanical properties of concrete under a dynamic strain rate can be significantly different from those under the static strain rate [17-20]. According to previous studies on the strain rate effect of concrete, it is generally concluded that the compressive strength, tensile strength and elastic modulus are all improved gradually with the increase of strain rate, and the compressive strength is less affected by the strain rate than the tensile strength [3, 21, 22]. However, the conclusions on the peak strain of concrete are contradictory [3, 23, 24]. Regarding the mechanism underlying the strain rate effect, a number of explanations have been reported from different perspectives [25-28], among which, the evolution of cracks, the viscosity effect, and the inertia effect were most widely discussed. Zhang et al. [29] employed a split Hopkinson pressure bar (SHPB) with a diameter of 75 mm to investigate the effects of strain rate, fiber type, and hybrid fiber content on the dynamic mechanical properties of basalt–polypropylene fiber-reinforced coral aggregate concrete (HBPRCAC) under impact loading. The results indicate that the incorporation of basalt fibers (BF) and polypropylene fibers (PF), particularly when used as hybrid fibers, effectively mitigates the damage to HBPRCAC. As the strain rate increases, the degree of damage intensifies; even at low strain rates, cracks propagate directly through the coral aggregates. At low strain rates, BF and PF are more prone to pull-out failure, whereas at high strain rates, they predominantly exhibit fracture failure.

The currently-available literature concerning the size effect on the mechanical properties of concrete under dynamic strain rates was usually based on the developing trend of compressive strength [3, 22, 30, 31]. Yu et al. [3] examined how the compressive strength of shale ceramsite lightweight aggregate concrete changed under the influence of size effect by considering different dynamic strain rates. The results suggested that the strain rate sensitivity was gradually weakened with the increase of size, and this trend was more obviously seen in shale ceramsite lightweight aggregate concrete than in ordinary concrete. Li et al. [22] conducted compression tests on nuclear power containment concrete with 3 different sizes by considering 10 different strain rates. It was found that the failure of concrete mainly occurred at the interface layer under a lower strain rate, while under a higher strain rate, the failure mode involved damage of coarse aggregates. Therefore, the size effect had a greater impact on the mechanical behaviors of nuclear containment structure under a higher strain rate. Jin et al. [11] established a mesoscopic model to numerically analyze the dynamic size effect of concrete under the strain rate from 10^{-5}/s to 200/s, and detected a critical strain rate in this range. When the loading strain rate was greater than the critical value, the size sensitivity of compressive strength would increase with the increase of strain rate; when the loading strain rate was lower than the critical value, the size sensitivity of compressive strength would decrease with the increase of strain rate. Xu et al. [32] employed a split Hopkinson pressure bar (SHPB) system to investigate the dynamic mechanical response of steam-cured concrete under different strain rates. The results indicate that the effect of curing temperature on strength exhibits a trend of first increasing and then decreasing. Furthermore, under dynamic loading, the enhancing effect of strain rate on strength is greater than that of curing temperature.

However, analyses on the compressive failure mode of concrete under the strain rate effect and size effect were usually based on the failure morphology upon the completion of loading action, while the evolution of cracks during the full-stage failure process was rarely examined. Moreover, there are few studies focusing on the developing trend of the full compressive curve under the coupling influence of size effect and strain rate effect. Up to date, research on the mechanical parameters under the strain rate effect mainly focuses on the compressive strength and tensile strength. No systematic

studies on other mechanical characteristic values, such as the loading curve changing trend, the crack evolution trend, the energy absorption characteristics and concrete damage, have been reported yet.

Based on the literature review above, uniaxial compression tests were carried out on fly ash concrete in this paper to explore the developing trends of various mechanical properties under the influence of strain rate effect and size effect. During the experiment, high-speed cameras were used to record the development of crack failure during the entire compression process in order to analyze the crack evolution process under different working conditions. Then, based on statistical analyses of various mechanical parameters (e.g., compressive strength, peak strain, elastic modulus and energy absorption) obtained from the experiment, a semi-empirical, semi-theoretical model for simulating the developing trend of the stress-strain curve of fly ash concrete under the coupling influence of strain rate effect and size effect was established. The research outcome of this study provides a theoretical basis for the application and development of fly ash concrete in civil and hydraulic engineering.

1. Experiment overview

1.1 Sample preparation

In this paper, the samples of fly ash concrete were designed with a strength grade of 35MPa, and the specific mix ratio was determined according to the "Technical code for application of fly ash concrete (GBT50146-2014)" . The raw materials include cement, water, fine aggregates, coarse aggregates, fly ash and water reducing agent (their masses in each cubic meter of mixture are 340kg, 170kg, 735kg, 1070kg, 85kg and 4.25kg, respectively). More specifically, the cement is ordinary Portland cement P.O 42.5; the coarse aggregates are continuous graded natural aggregate crushed stone with a particle size of 5-20mm and an apparent density of 2700kg/m3; the fine aggregates are river sand with a fineness modulus of 2.5 and an apparent density of 2650kg/m3; the fly ash is Grade II fly ash with a loss on ignition of 2.6%, a moisture content of 0.2% and a stability of 1.5mm; the water reducing agent is the potassium naphthalene sulfonate condensate water reducing agent (for 1.0%-2.0% of the cement mass, the corresponding water reducing efficiency is 20%-30%). The concrete blocks used in the experiment were poured according to the mix ratio above, and were then cured under room temperature (20±3 ℃) and 95% humidity for 28 days. Many recent studies have shown that the secondary hydration of fly ash is a "slow" and "persistent" process, requiring more than 90 days or even 180 days to significantly affect the concrete microstructure [33]. Therefore, the specimens were then immersed in a natural environment for 120 days to allow the fly ash to fully react.

In this paper, cylindrical samples of 3 different sizes (Φ50mm×100mm, Φ75mm×150mm and Φ100mm×200mm) were fabricated by the method of drilling core sampling from the concrete blocks prepared above. This method can not only eliminate the potential impact imposed by the plastering surface of direct pouring, but also ensure the flatness of the upper and lower surfaces and the verticality of the cylinder, so as to reduce the probability of eccentric compression to capture the actual axial compressive data.

1.2 Loading plan

To examine the coupling influence of size effect and strain rate effect on the mechanical properties of fly ash concrete, 3 sample sizes, namely large (L: Φ100mm×200mm), medium (M: Φ75mm×150mm) and small (S: Φ50mm×100mm), and 4 loading strain rates were considered in this study. It is well known that the strain rates for conventional static loads, self-weight and long-term loads typically range from 1.0×10^{-6}/s to 1.0×10^{-4}/s, whereas the strain rates for seismic loads, strong wind loads and equipment vibration loads (which have the greatest impact on concrete structures) range from 1.0×10^{-3}/s to 1.0×10^{-2}/s. Whereas impact and explosion strain rates (10^{2}/s to 10^{6}/s) are relatively uncommon in most concrete structures. Therefore, this paper selects four strain rates for analysis: 1.0×10^{-5}/s, 1.0×10^{-4}/s, 1.0×10^{-3}/s and 1.0×10^{-2}/s. In view of the randomness and discreteness characteristics of concrete during sample fabrication, 4 samples were prepared for each loading condition in order to calculate the mean values for analysis to improve the accuracy of the test data.



Fig. 1. Experiment equipment.



Fig. 2. Sample processing.

The compression tests were performed by an electro-hydraulic servo machine as shown in Figure 1, which can switch between multiple loading methods including displacement control and load control. The machine is installed with high-precision load sensors and displacement sensors that are well compliant with the measurement requirements. The samples fabricated by the drilling core sampling method are shown in Figure 2. The loading process was implemented by a hybrid method.

Firstly, the load control method was applied at a loading rate of 10kN/min, and after reaching 20kN, the machine was unloaded to zero. This process was repeated for three times to eliminate the gap between the sample surface and the machine to improve the accuracy of the test data. Then, the formal loading process was started by applying the displacement control method according to the loading rates determined earlier, until the failure of the sample. In order to control the impact of friction between the machine and the sample surface on the test results, lubricating grease was applied on

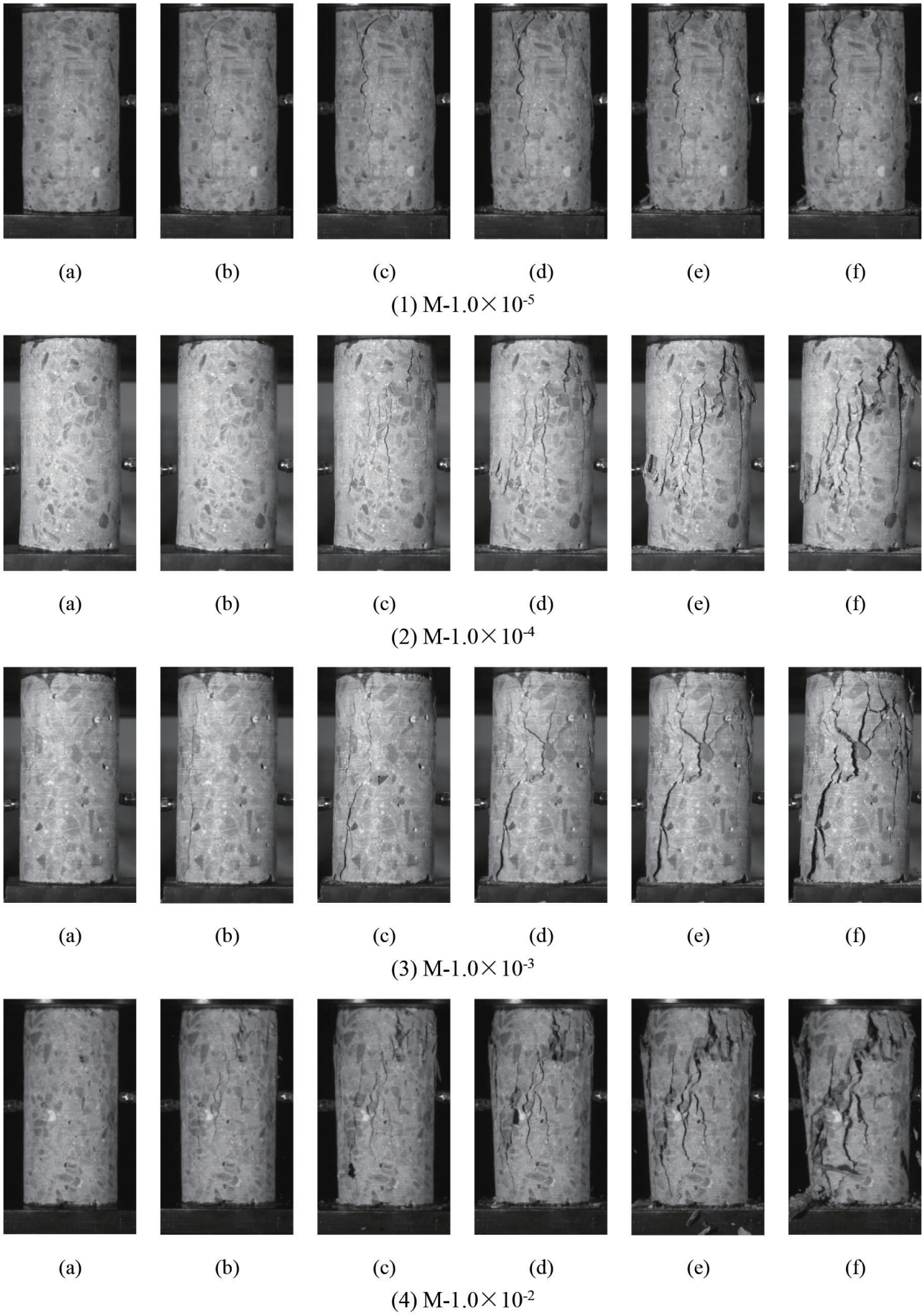


Fig. 3. Full process of failure evolution under different strain rates.

the contact surfaces by referring to Yu et al. [3]. This method can effectively reduce the impact of friction to improve the test accuracy. To better analyze the crack developing trend of fly ash concrete during the compression process, a high-speed camera was used to record the full-stage failure evolution throughout the entire loading process.

2. Analysis of test results

2.1 Failure evolution

According to the experiment plan above, the full-stage failure evolution images of fly ash concrete under different loading conditions were captured by the high-speed camera, and 6 typical time points were selected for comprehensive analysis. Then, the mechanical failure characteristics of fly ash concrete were examined from a macroscopic perspective based on the failure modes, as shown in Figure 3-4.

The influence of loading strain rate effect on the crack evolution of fly ash concrete under uniaxial compression was analyzed according to Figure 3. As it can be seen, under the static strain rate of 1.0×10^{-5}/s, the crack develops slowly, and the failure mode is mainly manifested as a single main crack. Except for the main crack, the integrity of other parts

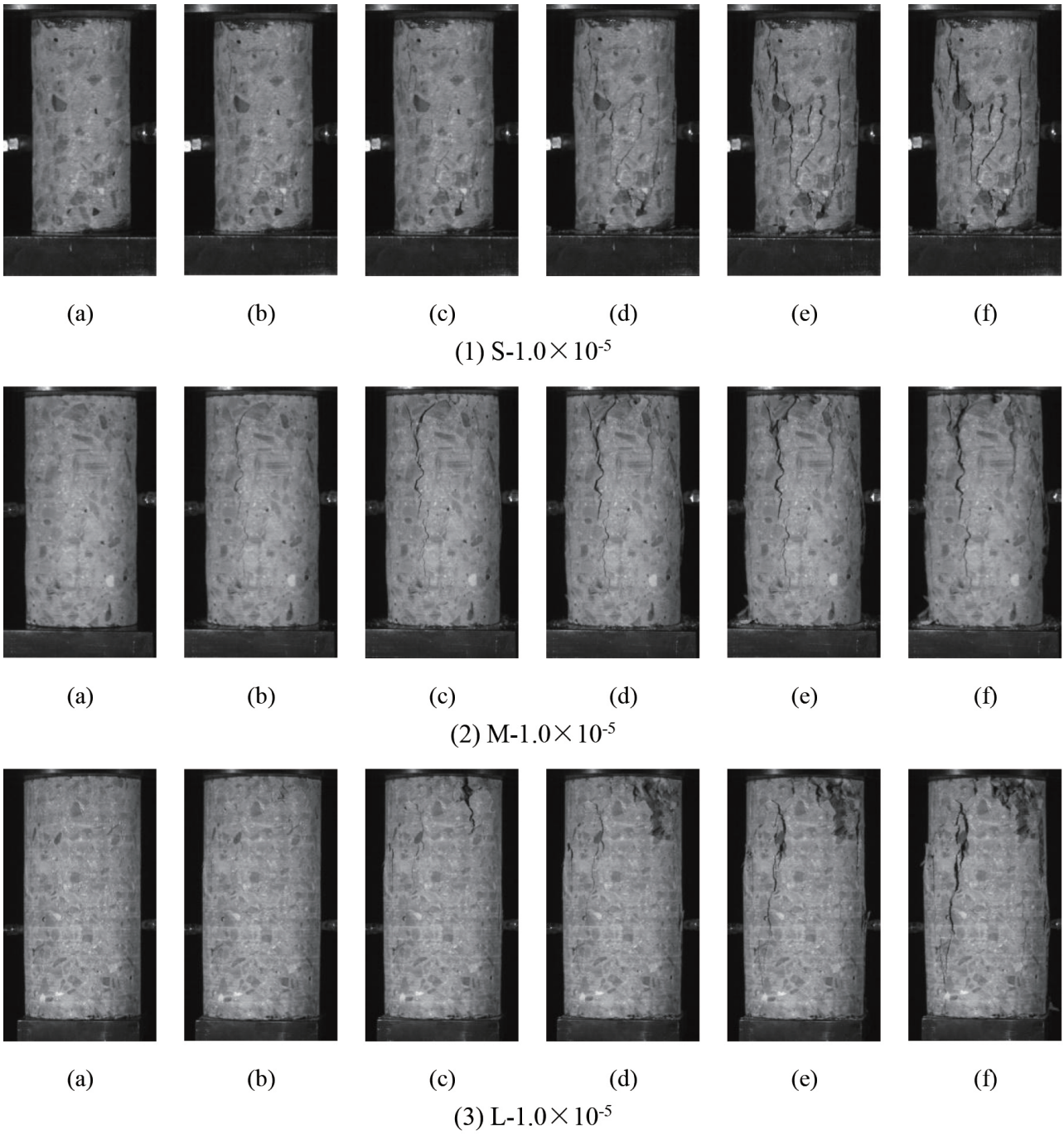


Fig. 4. Full failure evolution process of fly ash concrete with different sizes.

of the sample is generally good, without occurrence of any obvious cracking zone. The crack has a small width and mainly propagates along the interface between mortar and coarse aggregates. Affected by the distribution of aggregates, the development path of the crack shows a tortuous pattern. With the increase of strain rate, the propagation of the crack is gradually accelerated during the loading process, and multiple small cracks were generated concurrently. The small cracks expand and widen continuously, and the entire sample presents a serious deformation. As the loading time extends, a certain number of coarse aggregates are damaged accompanying with crack development. Upon failure, a large number of fragments are formed and peel off from the non-loaded surface. Overall, the compressive failure mode of fly ash concrete shows an obvious strain rate effect under different strain rates. The crack evolution process indicates that the failure of fly ash concrete occurs more suddenly and the damage is more serious under a higher strain rate.

The influence of size effect on the compressive failure mode of fly ash concrete was analyzed according to Figure 4. The compressive failure mechanism of fly ash concrete is similar to that of ordinary concrete, which is both attributed to horizontal tensile failure caused by the increase of horizontal tensile strain under the influence of vertical load and Poisson's ratio. The crack development pattern differs obviously among samples of different sizes. Specifically, the failure evolution of sample "S" is significantly different from that of the other two sizes. On the non-loaded surface of sample "S" , some fine and oblique cracks are formed, while the crack failure pattern on the non-loaded surface of the other two sizes is basically a single vertical crack penetrating the sample. The crack developing trend over time is also significantly different among different sizes. The single vertical crack on sample "L" appears earlier, and propagates and widens continuously with time, without generation of new cracks. However, on sample "S" , multiple small cracks are formed around the same time but in a relatively later stage, and the cracks develop rapidly. The compressive failure modes of fly ash concrete with different sizes are obviously different, thereby suggesting an obvious size effect.

In order to further explore the influence of strain rate effect and size effect on the compressive properties of fly ash concrete, the compressive failure morphologies under the strain rate effect and size effect were summarized based on the full-stage failure evolution process under different loading conditions (Figure 5-6).

From Figure 3, it can be seen that the loading process takes a longer time under a lower strain rate, so that the interior of the sample is subjected to uniform stress and the crack can be fully developed. Accordingly, the stress has sufficient time to find the weakest path in the sample to form micro-cracks. Since the weak areas are generally distributed around the interface layer between the cement mortar and coarse aggregates, the failure mode under a lower strain rate is mainly manifested as interface slip failure. As the loading strain rate grows, the failure process is gradually shortened, so that the compressive stress can no longer be evenly distributed throughout the entire sample. Consequently, the internal stress cannot uniformly and fully transmit. Moreover, the addition of fly ash can improve the compactness and reduce the weak areas in the concrete, so that the micro-cracks can develop rapidly to penetrate and damage coarse aggregates to release the concentrated energy. Therefore, the fracture effect of coarse aggregates can be more obviously observed under a higher strain rate, as shown in Figure 5. For a larger-sized sample, the ratio of the average volume of coarse aggregates to the volume of the entire sample (referred to as the coarse aggregate volume ratio in this paper) is smaller. Thus, the crack is more prone to developing along the weak path around the interface layer. For a smaller-sized sample, the coarse aggregate volume ratio is greater, so that the crack cannot easily bypass coarse aggregates during its evolution process. In the end, more tortuous cracks will be formed upon compressive failure in order to release energy, as shown in Figure 6.

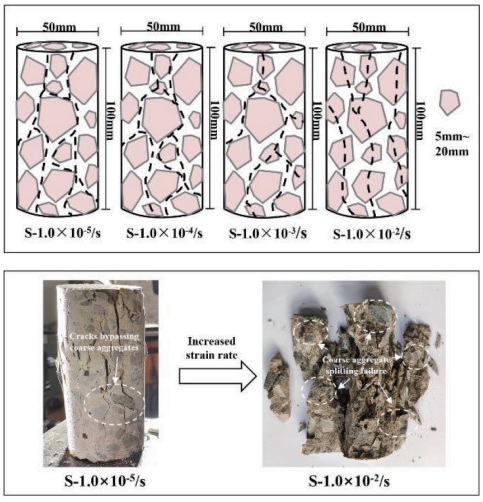


Fig. 5. Failure of aggregates of fly ash concrete under different strain rates.

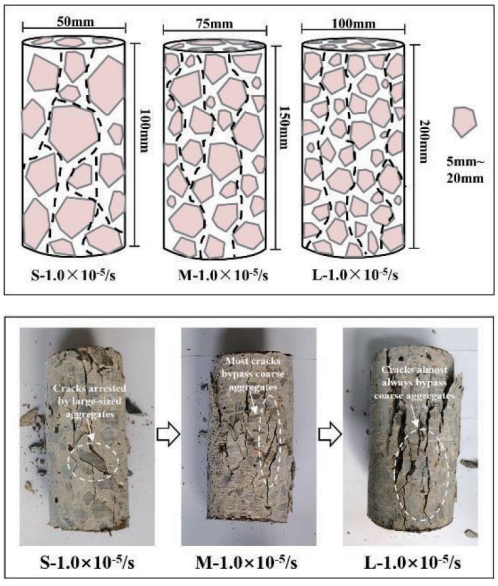


Fig. 6. Crack propagation of fly ash concrete under different coarse aggregate volume ratios.

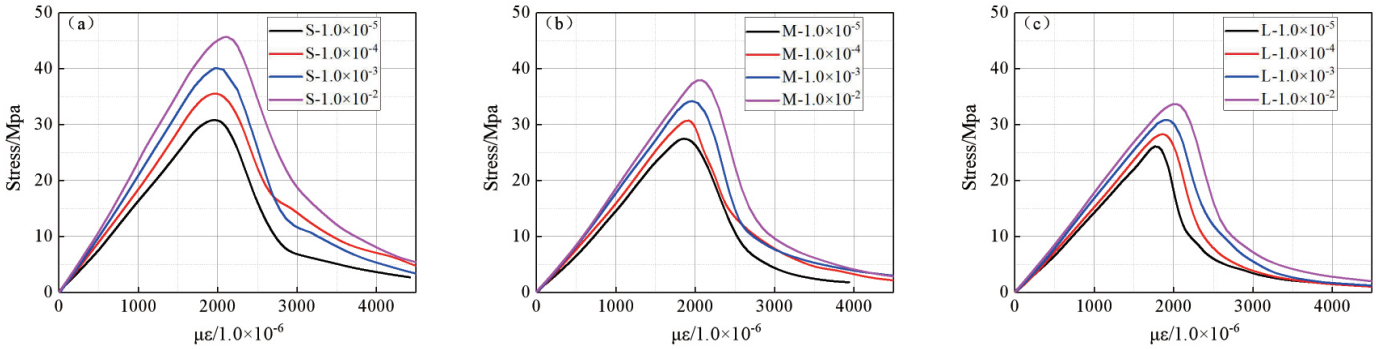


Fig. 7. The average stress-strain curve corresponding to different sizes and strain rates.

Comprehensive analysis on the coupling influence of strain rate effect and size effect suggests that, with the increase of strain rate, the failure mode of fly ash concrete will gradually transform from the pattern of a single main crack to the pattern of multiple cracks. Compared to the loading condition under a lower strain rate, the failure mode under a higher strain rate shows a higher degree of damage, accompanied by more cracks and more energy release. Such a failure developing trend under the influence of strain rate effect is more obviously observed in a smaller-sized sample.

2.2 Stress-strain curve

Based on data acquired by the computer-controlled electro-hydraulic servo machine, the stress-strain curve for each working condition of fly ash concrete was obtained as the average of 4 parallel tests, as shown in Figure 7.

According to the stress-strain curves under different strain rates as shown in Figure 7, the compressive strength of fly ash concrete shows an upward trend with the increase of strain rate. According to the slopes of the ascending and descending sections of the stress-strain curve under various working conditions, it can be seen that the elastic modulus increases gradually and the brittleness characteristics become more obvious as the strain rate grows.

The influence of size effect on the stress-strain curve can be summarized as follows. When the loading strain rate remains unchanged, the compressive strength and elastic modulus decrease gradually and the brittleness characteristics are gradually weakened with the increase of sample size. However, the peak strain shows a discrete trend with the increase of size. In order to further explore the influence of strain rate effect and size effect on the compressive properties of fly ash concrete, the developing trends of various mechanical properties under different working conditions will be examined more comprehensively in later sections.

2.3 Compressive strength

The dynamic increase factor αDIF, as shown in Equation (1), is often used in strength analysis of concrete in previous studies [3, 22, 34].

$$\alpha_{DIF} = \frac{\sigma_d}{\sigma_s} \quad (1)$$

Where, αDIF refers to the dynamic increase factor of compressive strength; σs refers to the concrete compressive strength under the static loading strain rate (1.0×10^{-5}/s, unit: MPa); σd refers to the concrete compressive strength under a dynamic loading strain rate (>1.0×10^{-5}/s, unit: MPa).

Figure 8 shows the relationship between the compressive strength and loading strain rate of fly ash concrete corresponding to 3 different sizes. As the strain rate grows, the compressive strength shows an obvious increasing trend. For sample "S" , the compressive strength increases from 30.81MPa to 45.66MPa, suggesting an improvement by 48.18%. For sample "M" , the compressive strength increases from 27.46MPa to 37.95MPa, suggesting an improvement by 38.19%. For sample "L" , the compressive strength increases from 26.09MPa to 33.67MPa, suggesting an improvement by 29.07%. The test results indicate that sample "L" has the smallest improvement in compressive strength due to the increase of strain rate. For all the 3 different sizes, the improvement in uniaxial compressive strength of fly ash concrete under the strain rate effect is higher than that of ordinary concrete as reported by Li et al. [22], which implies that the strain rate effect has a stronger impact on fly ash concrete. From a microscopic perspective, during the secondary hydration reaction of fly ash, the reactive SiO_2 and Al_2O_2 in the fly ash react with $Ca(OH)_2$ generated by cement hydration. This process not only consumes most of the $Ca(OH)_2$ but also produces substantial amounts of C-S-H (calcium silicate hydrate) gel and, in some cases, the more polymerized C-A-S-H (calcium aluminum silicate hydrate) gel. The newly formed gels act as a "binder" tightly cementing surrounding hydration products together, which significantly enhances the strength of the interfacial transition zone (ITZ) in fly ash concrete and reduces its internal porosity [35-37]. Consequently, this mitigates the tendency of cracks to bypass coarse aggregates under low strain rate conditions, thereby increasing the strain rate sensitivity of fly ash concrete. From the perspective of fracture mechanics, the unique micro-bead effect of fly ash forces crack propagation to consume more energy in penetrating the fly ash micro-beads and their dense hydration

products, which further corroborates the above observations.

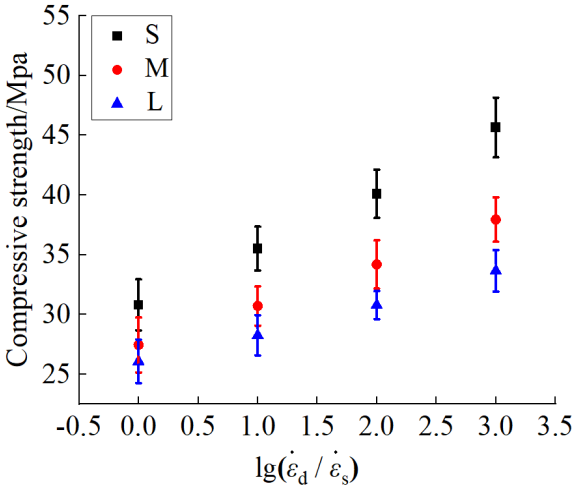


Fig. 8. Loading strain rate and compressive strength of fly ash concrete.

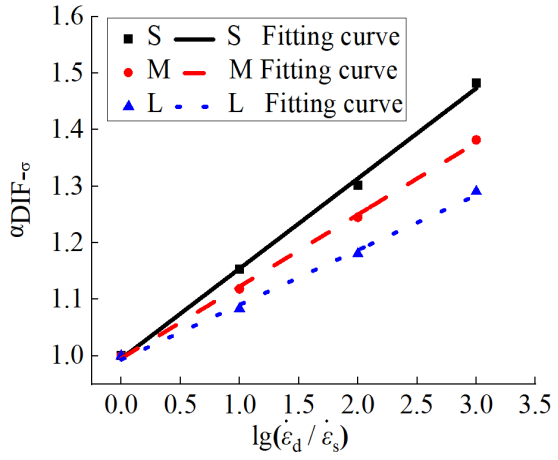


Fig. 9. Loading strain rate and the dynamic increase factor of compressive strength.

Then, the developing trend of compressive strength under the influence of strain rate effect was quantitatively analyzed according to the relationship between the loading strain rate and the dynamic increase factor of compressive strength as shown in Figure 9. Li et al. [22] proposed the equation describing the relationship between the strain rate and the dynamic increase factor of compressive strength for ordinary concrete as shown in Equation

$$\alpha_{DIF} = b + a\lg(\varepsilon'_d / \varepsilon'_s) \quad (2)$$

A mass of studies [3, 22] have conducted mathematical regression analysis using Equation (2), and it has been concluded that the dynamic increase factor of compressive strength is linearly correlated with the dimensionless logarithm of strain rate. In Equation (2), the value of coefficient b is generally ranged between 0.98 and 1.02. Considering that b is the dynamic increase factor under the static loading condition, its value was set to 1 in this paper. Then, the equation for the relationship between the strain rate and the dynamic increase factor of comprehensive strength as shown in Equation (3) was obtained.

$$\alpha_{DIF} = 1 + a\lg(\varepsilon'_d / \varepsilon'_s) \quad (3)$$

Based on the test data of compressive strength under different loading strain rates for 3 different sizes of fly ash concrete, mathematical regression analysis was performed on Equation (3), and the regression curves as shown in Figure 9 and Equation (4)-(6) were obtained.

S:

$$\alpha_{DIF} = 1 + 0.159\lg(\varepsilon'_d / \varepsilon'_s) \quad R^2=0.99806 \quad (4)$$

M:

$$\alpha_{DIF} = 1 + 0.127\lg(\varepsilon'_d / \varepsilon'_s) \quad R^2=0.99897 \quad (5)$$

L:

$$\alpha_{DIF} = 1 + 0.097\lg(\varepsilon'_d / \varepsilon'_s) \quad R^2=0.99626 \quad (6)$$

From Figure 9 and Equation (4)-(6), it can be seen that the dynamic increase factor of compressive strength of fly ash concrete is linearly correlated with the dimensionless logarithm of strain rate for all the 3 different sample sizes. According to the compressive strength variation factor a of fly ash concrete under the strain rate effect for different sample sizes, it can be found that the value of a increases gradually with the decrease of size. The test data in this paper indicates that, when the strain rate is ranged from 1.0×10^{-5}/s to 1.0×10^{-2}/s, the smaller the sample size, the larger the increase of compressive strength under the strain rate effect is. This conclusion is basically consistent with the related reports on ordinary concrete under the coupling influence of size effect and strain rate effect in the same range of strain rate (1.0×10^{-5}/s – 1.0×10^{-2}/s) [3, 22].

Then, by further considering the variation of compressive strength of fly ash concrete under the size effect, the changing trend of compressive strength under the coupling influence of strain rate effect and size effect was obtained as shown in Figure 10 according to the dimensionless logarithm of different loading strain rates.

It can be seen from Figure 10 that, for the same strain rate, the compressive strength of fly ash concrete decreases gradually with the increase of size. As the strain rate grows, the changing range of compressive strength varies significantly under the influence of size effect. Under the static strain rate of 1.0×10^{-5}/s, the changing range of compressive strength is 2.36MPa under the influence of size effect. When the strain rate increases to 1.0×10^{-2}/s, the changing range of compressive strength is increased to 6.00MPa under the influence of size effect. This implies that the change of compressive strength under the influence of size effect is gradually enlarged as the strain rate grows. In order to further explore the developing trend of compressive strength affected by the size effect

under different strain rates, the relationship between the sample size and the compressive strength attenuation factor σ/σ50 was obtained as shown in Figure 11, where σ50 refers to the compressive strength of sample "S" , σ refers to the compressive strength of sample "M" (i.e., σ75) or sample "L" (i.e., σ100). The finding is consistent with the conclusion of Li et al. [22] that the changing range of compressive strength under the size effect is linearly correlated with the dimensionless logarithm of strain rate.

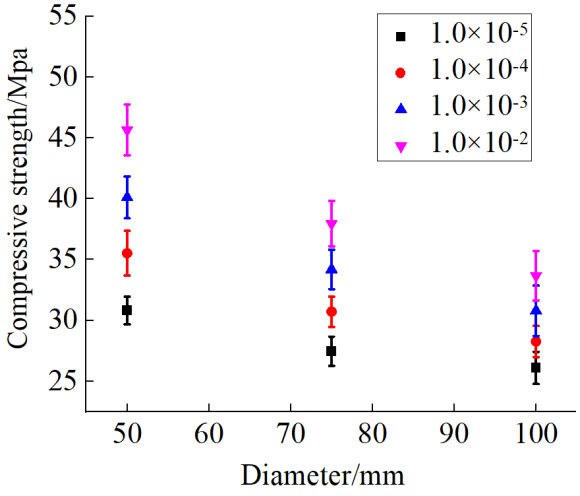


Fig. 10. Relationship between the size and compressive strength of fly ash concrete.

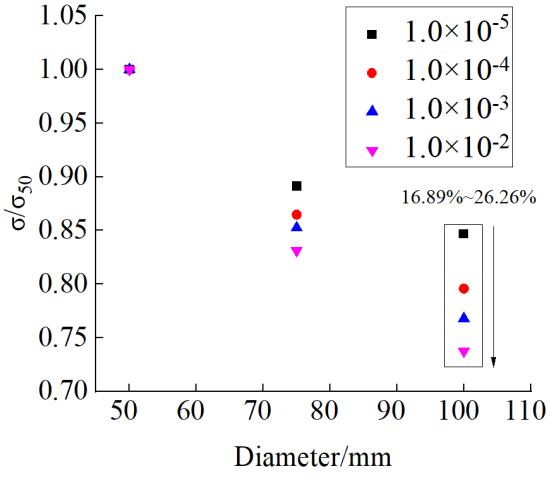


Fig. 11. Relationship between the size and the compressive strength attenuation factor of fly ash concrete.

According to Figure 11, when the loading strain rate remains constant, the compressive strength decreases gradually with the increase of size. For a strain rate ranged between 1.0×10^{-5}/s and 1.0×10^{-2}/s, the compressive strength of sample "L" is reduced by 16.89% – 26.26% compared to that of sample "S" . The overall developing trend indicates that the reduction in compressive strength under the size effect is gradually enlarged as the strain rate grows. By considering the strain rate in the same range, Li et al. [22] reported that, the compressive strength of 70mm cubic concrete sample increased from 35.92MPa to 47.09MPa under the influence of strain rate, suggesting an improvement by 31.09%, and the compressive strength of 100mm cubic sample increased from 31.14MPa to 36.24MPa under the influence of strain rate, suggesting an improvement by 16.38%. Comparative analysis shows that the influence of size effect on the compressive strength of fly ash concrete is stronger than that on ordinary concrete. Research on the relationship between size effect and compressive strength is usually carried out based on quantitative analysis from two perspectives, the size effect degree and the size effect law. For instance, Bazant [13] proposed the size effect equation for concrete compressive strength from the perspective of size effect law, as shown in Equation (7).

$$\sigma_N = \sigma_\infty\left(1+\frac{D_b}{D}\right) \tag{7}$$

Where, σ_N refers to the nominal compressive strength corresponding to any size of concrete sample; $\sigma\ \infty$ refers to the nominal compressive strength corresponding to an infinitely-large sample; D_b refers to the structural characteristic dimension of the sample; D refers to the diameter of the sample. For the convenience of analysis, the parameter σ_N in Equation (8) was non-dimensionalized based on σ50, and eventually, the expression of size effect law as shown in Equation (8) was obtained, where c_σ refers to the dimensionless value of the nominal compressive strength corresponding to an infinitely-large sample.

$$\frac{\sigma_N}{\sigma_{50}} = \frac{\sigma_\infty}{\sigma_{50}}\left(1+\frac{D_b}{D}\right) = c_\sigma\left(1+\frac{D_b}{D}\right) \tag{8}$$

According to the equation of size effect law as shown in Equation (8), mathematical regression was performed on the compressive strength of fly ash concrete with 3 different sample sizes under 4 different strain rates, and the expression of size effect law as shown in Figure 12 was obtained.

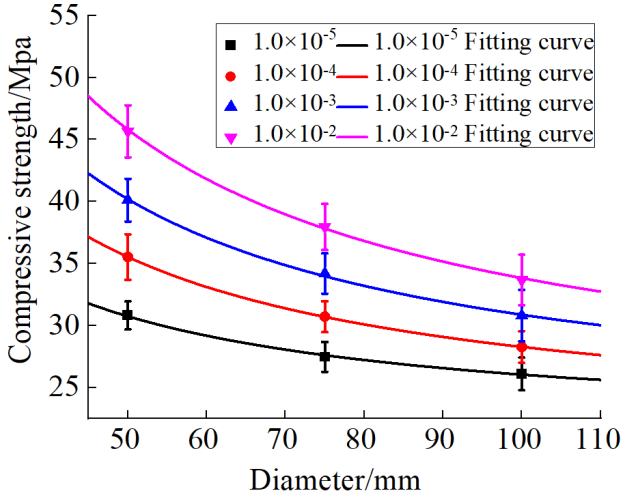


Fig. 12. Relationship between the size and compressive strength of fly ash concrete.

It can be seen from Figure 12 that the equation of size effect law has good applicability in describing the influence of size effect on the compressive strength of fly ash concrete

under different strain rates. Then, the strain rate effect on cσ and D_b was examined by performing statistical analysis on the relevant test data, as shown in Figure 13.

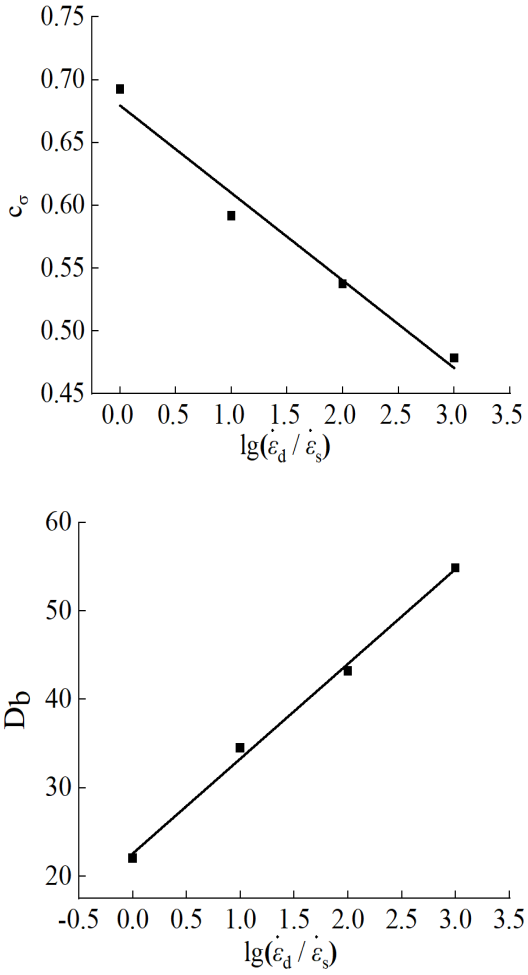


Fig. 13. Relationships between the size effect law parameters c_σ and D_b and the loading strain rate.

It can be seen from Figure 13 that c_σ decreases gradually while D_b increases gradually with the increase of the dimensionless logarithm of loading strain rate. By performing mathematical regression analysis on these parameters, the relationships between c_σ and D_b and the loading strain rate were obtained, as shown in Equation (9)-(10).

$$c_\sigma = 0.6795 - 0.06969\lg(\varepsilon_d'/\varepsilon_s') \qquad R^2=0.97711 \quad (9)$$

$$D_b = 22.579 + 10.7164\lg(\varepsilon_d'/\varepsilon_s') \qquad R^2=0.99583 \quad (10)$$

By substituting Equation (9)-(10) into Equation (8), Equation (11) was obtained.

$$\sigma_N = \sigma_{50}\times\left[0.6795 - 0.06969\lg(\varepsilon_d'/\varepsilon_s')\right]\times\left[1+\frac{22.579+10.7164\lg(\varepsilon_d'/\varepsilon_s')}{D}\right] \qquad (11)$$

From Figure 12 and Equation (11), it can be seen that the compressive strength and size sensitivity of fly ash concrete are reduced gradually with the increase of size. When the sample size is larger than a threshold value, the further increase of size will have little impact on the compressive strength, and this threshold value is referred to as the critical dimension D_{cr}. The comprehensive strength corresponding to D_{cr} is known as the critical strength f_{cr}. When the sample size is larger than the critical dimension, the size effect of concrete can be ignored.

From Equation (11), the critical dimension D_{cr} and the critical strength fcr of fly ash concrete under different loading strain rates were calculated, based on which, the relationships between the loading strain rate and D_{cr} and f_{cr} were obtained, as shown in Figure 14.

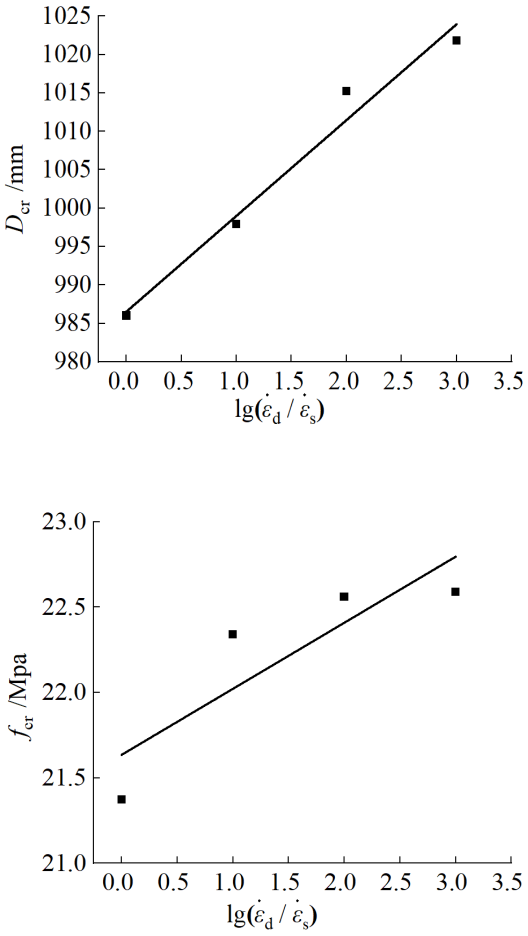


Fig. 14. Relationships between the loading strain rate and D_{cr} and f_{cr}.

According to Figure 14, the critical dimension and critical strength of fly ash concrete are linearly correlated with the dimensionless logarithm of strain rate. Based on qualitative analysis, mathematical regression was then performed on the calculation results, and the relationship equations as shown in Equation (12)-(13) were obtained.

$$D_{cr} = 986.52 + 12.47\lg(\varepsilon_d'/\varepsilon_s') \qquad R^2=0.97494 \quad (12)$$

$$f_{cr} = 21.635 + 0.387\lg(\varepsilon_d'/\varepsilon_s') \qquad R^2=0.76045 \quad (13)$$

Then, the parameter 21.635 in Equation (13) was used to non-dimensionalize the parameter 0.387, and the equation for the dynamic increase factor at the critical compressive strength fcr was obtained, as shown in Equation (14).

$$\alpha_{cr\text{-}DIF} = 1 + 0.01789 \lg(\varepsilon_d' / \varepsilon_s') \quad (14)$$

By comparing the slope in Equation (14) (i.e., 0.01789) with the slopes in Equation (4)-(6) (i.e., 0.159 for sample "S" , 0.127 for sample "M" , 0.097 for sample "L"), it can be found that the compressive strength is obviously affected by the loading strain rate when the sample reaches the critical dimension.

Since σ_{50} in Equation (11) represents the compressive strength of sample "S" under 4 different loading strain rates in the range from 1.0×10^{-5}/s to 1.0×10^{-2}/s, σ_{50} can be seen as a relational function of compressive strength with respect to the strain rate. By combining Equation (1) and Equation (4), Equation (15) was obtained, which could be further simplified to Equation (16). It is the equation describing the influence of strain rate effect on the compressive strength for sample "S" .

$$\frac{\sigma_{d\text{-}50}}{\sigma_{s\text{-}50}} = \alpha_{DIF} = 1 + 0.159 \lg(\varepsilon_d' / \varepsilon_s') \quad (15)$$

$$\sigma_{d\text{-}50} = \sigma_{s\text{-}50} + \sigma_{s\text{-}50} 0.159 \lg(\varepsilon_d' / \varepsilon_s') \quad (16)$$

Where, σs-50 refers to the compressive strength of sample "S" under static load (unit: MPa); $\sigma_{d\text{-}50}$ refers to the compressive strength of sample "S" under a dynamic load (unit: MPa).

By substituting σ_{50} in Equation (11) with Equation (16), Equation (17) was obtained. Thus, the equation describing the coupling influence of size effect and strain rate effect on the compressive strength of fly ash concrete was established.

$$\sigma_N = \frac{[\sigma_{s\text{-}50} + \sigma_{s\text{-}50} 0.159 \lg(\varepsilon_d' / \varepsilon_s')] \times [0.6795 - 0.06969 \lg(\varepsilon_d' / \varepsilon_s')]}{D / [D + 22.579 + 10.7164 \lg(\varepsilon_d' / \varepsilon_s')]} \quad (17)$$

2.4 Elastic modulus

Elastic modulus is one of the important parameters for describing the elastic deformation of concrete, and is a critical factor to be considered for establishing the empirical model. In this section, the developing trend of elastic modulus (which is defined as the secant modulus at 50% of the peak stress) of fly ash concrete under the coupling action of strain rate effect and size effect was statistically analyzed.

In order to comprehensively examine the coupling influence of strain rate effect and size effect on the peak strain, the dynamic increase factor of elastic modulus DIF_E (similar to the dynamic increase factor of comprehensive strength) was introduced, as shown in Equation (18).

$$DIF_E = \frac{E_d}{E_s} \quad (18)$$

Where, DIF_E refers to the dynamic increase factor of elastic modulus; Es refers to the elastic modulus under the static strain rate (1.0×10^{-5}/s, unit: 1×10^3MPa); Ed refers to the elastic modulus under a dynamic strain rate (>1.0×10^{-5}/s, unit: 1×10^3MPa).

According to the relationship between the elastic modulus and loading strain rate for 3 different sample sizes as shown in Figure 15, it can be seen that the elastic modulus has high sensitivity to strain rate. For sample "S" , the peak strain increases from 1.65×10^4MPa under the static strain rate of 1×10^{-5}/s to 2.30×10^4MPa under the strain rate of 1×10^{-2}/s, suggesting an increase by 39.40%. For sample "M" , the peak strain increases from 1.53×10^4MPa to 1.93×10^4MPa under the strain rate effect, suggesting an increase by 26.14%. For sample "L" , the peak strain increases from 1.48×10^4MPa to 1.78×10^4MPa under the strain rate effect, suggesting an increase by 20.27%. In general, the elastic modulus of fly ash concrete increases gradually with the increase of strain rate. For different sample sizes, the elastic modulus becomes more sensitive to the strain rate with the decrease of size. As shown in Figure 16, DIF_E exhibits an obvious upward trend as the strain rate grows. From the overall trend, it can be seen that the increase in elastic modulus under the strain rate effect is gradually reduced with the increase of size.

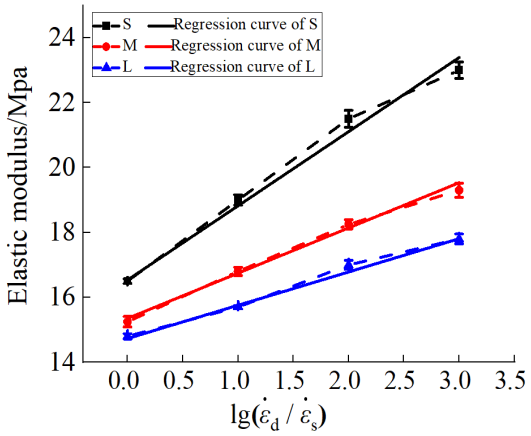


Fig. 15. Loading strain rate and elastic modulus of fly ash concrete.

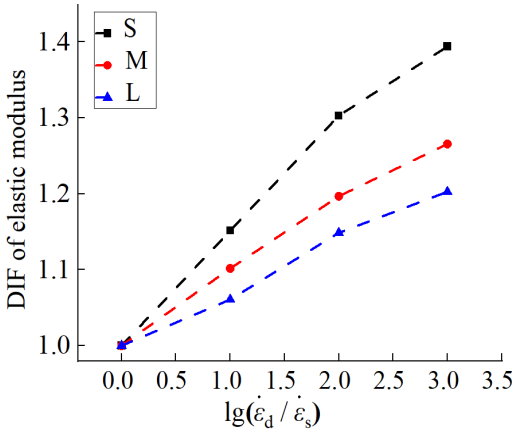


Fig. 16. Loading strain rate and the dynamic increase factor of elastic modulus.

In order to quantitatively reflect the developing trend of elastic modulus, mathematical regression was performed on Equation (19) using the data points of elastic modulus under different strain rates. Then, the mathematical regression curve as shown in Figure 15 and the fitting equations as shown in Equation (20)-(22) were obtained.

$$E = b + k\lg(\varepsilon_d'/\varepsilon_s') \quad (19)$$

Where, E refers to the elastic modulus (unit: 1×103MPa); b and k are parameters of the fitting equation, which can be determined by mathematical regression.

S:

$$E = 16.70 + 2.20\lg(\varepsilon_d'/\varepsilon_s') \quad (20)$$

M:

$$E = 15.36 + 1.36\lg(\varepsilon_d'/\varepsilon_s') \quad (21)$$

L:

$$E = 14.78 + 1.03\lg(\varepsilon_d'/\varepsilon_s') \quad (22)$$

Since Equation (20)-(22) only reflect the developing trend of elastic modulus with the change of strain rate for a particular size, in order to explore the changing trend of peak strain under the coupling influence of size effect and strain rate effect, statistical analysis was performed on b and k. The developing trends of b and k with the change of size are shown in Figure 17.

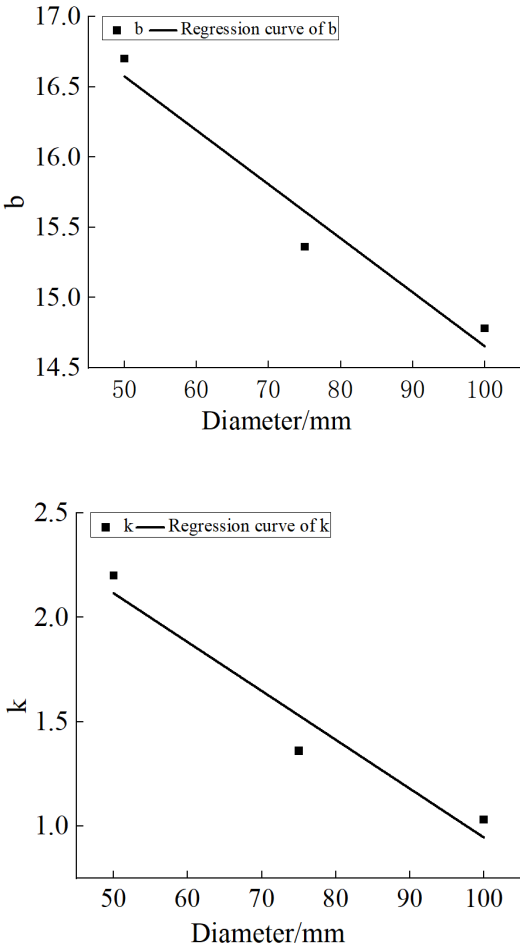


Fig. 17. Changing trends of parameter *b* and *k* with size.

According to Figure 17, the fitting equations for b and k were obtained by mathematical regression, as shown in Equation (23)-(24).

$$b = 18.49 - 0.0384D \quad (23)$$

$$k = 3.285 - 0.0234D \quad (24)$$

By substituting Equation (23)-(24) into Equation (19), the model equation describing the elastic modulus of fly ash concrete under the coupling influence of size effect and strain rate effect was proposed, as shown in Equation (25).

$$E = 18.49 - 0.0384D + (3.285 - 0.0234D)\times\lg(\varepsilon_d'/\varepsilon_s') \quad (25)$$

2.5 Energy absorption characteristics

For compression tests under a constant strain rate, the stress-strain curves obtained from multiple parallel tests show a certain degree of discreteness, which means it is not reasonable to simply compute the average stress-strain curve for analysis [38]. Therefore, in this paper, the stress-strain curve with the intermediate compressive strength among the 4 curves obtained for each working condition was selected to examine the compressive strength, compaction strain and energy absorption of fly ash concrete.

Miltz et al. [39] proposed to use the energy absorption efficiency E_f to evaluate the energy absorption characteristics of a material, as shown in Equation (26).

$$E_f(\varepsilon_a) = \frac{1}{\sigma_a}\int_0^{\varepsilon_a}\sigma(\varepsilon)d\varepsilon \quad (26)$$

Where, σ(ε) refers to the stress-strain functional relationship that describes a material under compression; ε_a is an arbitrary strain; σ_a is the stress corresponding to ε_a.

The optimal working state of energy absorption refers to the state when the energy absorption efficiency of a material reaches the maximum value. The strain corresponding to the maximum energy absorption efficiency is referred to as the compaction strain ε_D [40]. Usually, there are two or more maximum values of energy absorption efficiency for each sample, so it is necessary to comprehensively determine the value of ε_D based on the developing trend of the stress-strain curve. For the convenience of calculation, the peak strain εpk was used in this paper to replace the compaction strain ε_D, and the specific energy absorption W(J/cm3) was used to evaluate the energy absorption characteristics of fly ash concrete. W refers to the energy absorption capacity of fly ash concrete per unit volume, which can be computed by Equation (27).

$$W = \int_0^{\varepsilon_{pk}}\sigma(\varepsilon)d\varepsilon \quad (27)$$

Where, ε_{pk} refers to the peak strain of concrete; σ(ε) is a function of stress with respect to strain; ε is the strain value of concrete; W is the specific energy absorption (unit: J/cm3).

In order to comprehensively analyze the coupling influence of strain rate effect and size effect on the specific energy absorption, the dynamic increase factor of specific energy

absorption DIFW (similar to the dynamic increase factor of comprehensive strength) was introduced, as shown in Equation (28).

$$DIF_W = \frac{W_d}{W_s} \tag{28}$$

Where, DIF_W refers to the dynamic increase factor of concrete specific energy absorption; Ws refers to the specific energy absorption under the static loading strain rate (1.0×10^{-5}/s, unit: J/cm3); W_d refers to the specific energy absorption under a dynamic loading strain rate (>1.0×10^{-5}/s, unit: J/cm3).

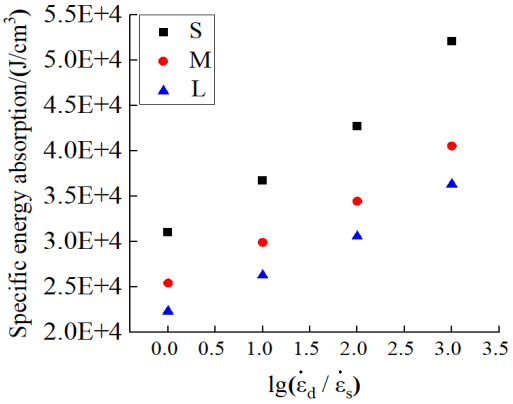


Fig. 18. Loading strain rate and specific energy absorption rate of fly ash concrete.

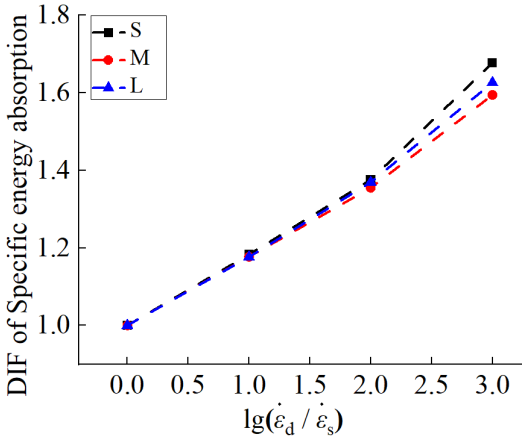


Fig. 19. Loading strain rate and the dynamic increase factor of specific energy absorption rate.

According to Equation (27), the values of W with the change of sample size and strain rate were calculated and sorted out, as shown in Figure 18. It can be seen that the specific energy absorption rate of fly ash concrete shows an obvious strain rate effect. As the strain rate grows, the energy absorption capability of fly ash concrete is strengthened gradually in a roughly linear manner. From Figure 19, the relationship between the dynamic increase factor of specific energy absorption rate and the loading strain rate also forms a roughly linear function, and it is not obviously affected by the size effect.

In summary, the specific energy absorption of fly ash concrete is gradually increased with the increase of strain rate. In the initial loading stage, most of the energy input by the testing machine is stored in the sample in the form of elastic strain energy. As the load grows, the plastic deformation energy will exceed the elastic strain energy under a higher strain rate, and the energy of the sample is mostly released in the form of fracture surface energy, frictional heat energy and plastic deformation energy. Since the energy release is greatly reduced, the sample exhibits a ductile failure mode. On the contrary, the elastic strain energy of the sample is higher than the plastic deformation energy under a lower strain rate. Since the sample has accumulated a lot of energy during the elastic stage, once the storage limit is reached, the energy will be rapidly released to result in brittle failure. With the decrease of sample size, the specific energy absorption of fly ash concrete shows a continuously-growing trend. This is mainly because, under the influence of aggregate volume ratio, the crack developing path penetrating through a smaller-sized sample appears to be more tortuous, and the specific energy absorption is greater, which reflects a stronger absorption capability.

2.6 Statistical analysis

For the developing trend of the stress-strain curve of concrete, Weibull [41] proposed the brittle failure theory based on the “weakest chain” concept, which emphasizes that the strength of the weakest link in the chain determines the failure load of the entire chain. This theory can well simulate the stress-strain developing trend of traditional concrete structures before reaching the peak stress. For simulating the stress-strain curve after reaching the peak stress, the Lognormal distribution theory can be applied. By using this method, a piecewise constitutive equation of concrete was obtained, as shown in Equation (29).

$$\sigma = \begin{cases} E\varepsilon \cdot \exp[-m(\frac{\varepsilon}{\varepsilon_{pk}})^{\frac{1}{m}}] & 0 \le \varepsilon \le \varepsilon_{pk} \\ \sigma_{pk} \cdot \exp\{-0.5[\frac{\ln(\varepsilon/\varepsilon_{pk})}{t}]^2\} & \varepsilon \ge \varepsilon_{pk} \end{cases} \tag{29}$$

Where, εpk refers to the peak strain (unit: 1×10^{-3}); σ_{pk} refers to the peak stress (unit: MPa); E refers to the elastic modulus (unit: MPa); m is the curve shape parameter of the ascending section $m=\ln((E\varepsilon_{pk})/\sigma_{pk})$; t is the shape control parameter of the descending section, which can be obtained by mathematical regression.

The changing trend of t with size can be obtained by mathematical regression, as shown in Equation (30):

$$t = 0.32 - 0.0016D \tag{30}$$

There has been no consistent conclusion with respect to the influence of dynamic size effect on the peak strain of concrete [3, 18, 19]. By referencing to the analysis method for compressive strength, the coupling influence of strain rate effect and size effect on the peak strain of fly ash concrete is illustrated in Figure 20.

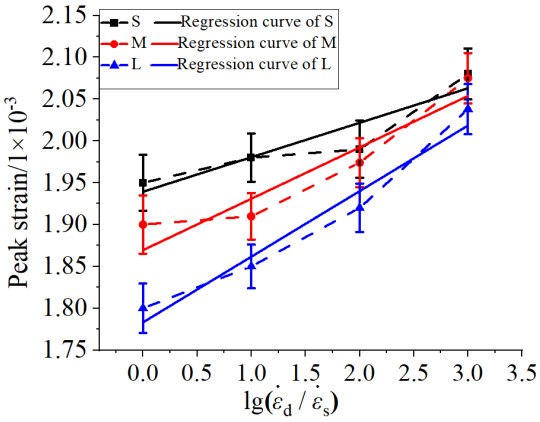


Fig. 20. Loading strain rate and peak strain of fly ash concrete.

According to the relationship between the peak strain and loading strain rate for 3 different sample sizes as shown in Figure 20, it can be seen that the peak strain shows a tortuous developing trend with the increase of strain rate. For sample "S" , the peak strain increases from 1.948×10^{-3} under the static strain rate of 1×10^{-5}/s to 2.081×10^{-3} under the strain rate of 1×10^{-2}/s, suggesting an increase by 6.83%. For sample "M" , the peak strain increases from 1.909×10^{-3} to 2.075×10^{-3} under the strain rate effect, suggesting an increase by 8.70%. For sample "L" , the peak strain increases from 1.788×10^{-3} to 2.038×10^{-3} under the strain rate effect, suggesting an increase by 13.98%. Similar to the analysis method on compressive strength, the equation describing the coupling influence of size effect and strain rate effect on the peak strain of fly ash concrete was obtained by performing mathematical regression on the peak strain, as shown in Equation (31).

$$\varepsilon = 2.1000 - 0.003D + (0.0015 + 0.0008D) \times \lg(\dot{\varepsilon}_d' / \dot{\varepsilon}_s') \tag{31}$$

Then, by substituting the compressive strength fitting Equation (17), the elastic modulus fitting Equation (25), the parameter t fitting Equation (30) and the peak strain fitting Equation (31) into Equation (29), Equation (32) and Equation (33) were obtained:

$$\sigma\begin{cases} \left[18.49-0.038D+3.29\lg(\dot{\varepsilon}_d'/\dot{\varepsilon}_s')-0.02D\lg(\dot{\varepsilon}_d'/\dot{\varepsilon}_s')\right]\cdot\varepsilon\cdot\exp\left\{-m\left[\dfrac{10000\varepsilon}{21000-30D+(15+8D)\cdot\lg(\dot{\varepsilon}_d'/\dot{\varepsilon}_s')}\right]^{\frac{1}{m}}\right\} & 0\le\varepsilon\le\varepsilon_{pk} \\ \dfrac{\left[\sigma_{s\text{-}50}+\sigma_{s\text{-}50}0.16\lg(\dot{\varepsilon}_d'/\dot{\varepsilon}_s')\right]\cdot\left[0.68-0.07\lg(\dot{\varepsilon}_d'/\dot{\varepsilon}_s')\right]}{D/\left[D+22.58+10.7\lg(\dot{\varepsilon}_d'/\dot{\varepsilon}_s')\right]}\cdot\exp\left\{\dfrac{-5000}{(32-0.16D)^2}\cdot\left[\ln\left(\dfrac{10000\varepsilon}{21000-30D+(15+8D)\cdot\lg(\dot{\varepsilon}_d'/\dot{\varepsilon}_s')}\right)\right]^2\right\} & \varepsilon\ge\varepsilon_{pk} \end{cases} \tag{32}$$

$$m=\ln\left(\frac{\left[18.49-0.0384D+(3.285-0.0234D)\cdot\lg(\dot{\varepsilon}_d'/\dot{\varepsilon}_s')\right]\cdot\left[21000-30D+(15+8D)\times\lg(\dot{\varepsilon}_d'/\dot{\varepsilon}_s')\right]}{10000\cdot\dfrac{\left[\sigma_{s\text{-}50}+\sigma_{s\text{-}50}0.16\lg(\dot{\varepsilon}_d'/\dot{\varepsilon}_s')\right]\cdot\left[0.68-0.07\lg(\dot{\varepsilon}_d'/\dot{\varepsilon}_s')\right]}{D/\left[D+22.58+10.7\lg(\dot{\varepsilon}_d'/\dot{\varepsilon}_s')\right]}}\right) \tag{33}$$

Further, the semi-empirical, semi-theoretical constitutive model considering the coupling influence of strain rate effect and size effect on the full-stage stress-strain curve of fly ash concrete was obtained by substituting the value of m in Equation (32) with Equation (33). There are three correlation parameters in this equation: $\lg(\dot{\varepsilon}_d/\dot{\varepsilon}_s)$ is the strain rate influencing factor; D is the dimension influencing factor (i.e., the diameter of the cylindrical sample in this paper, unit: mm); $\sigma_{s\text{-}50}$ is the compressive strength of sample "S" (Φ50mm×100mm) under the static load (unit: MPa).

The model equation established above was then used to simulate the performance of fly ash concrete with different sample sizes under different strain rates, and the simulation results were compared with the test data, as shown in Figure 21.

As shown in Figure 21, the established model has a high degree of fitting to the stress-strain curve of fly ash concrete under the coupling influence of strain rate effect and size effect. Moreover, for other types of concrete, the empirical constitutive model can be easily obtained by replacing the parameter equations in this model with appropriate ones. In view of its good applicability and variability, the model proposed in this paper is of an important theoretical significance for the development of empirical and constitutive models for other types of concrete.

3. Discussions

The full-stage compressive failure process can clearly reflect the strain rate effect on the compressive performance of fly ash concrete. Under a lower strain rate, there is enough time to redistribute the compressive stress throughout the entire sample, so that the stress can fully develop. Accordingly, the internal damage evolution shows a more uniform distribution pattern inside the entire sample. On the contrary, under a higher strain rate, there is not enough time to fully distribute the compressive stress throughout the entire sample, and the damage is largely concentrated in a local area. Consequently, the sample exhibits a severe and concentrated failure mode upon failure, and the damage evolution mainly takes place around the crack. Generally speaking, the strain rate effect of fly ash concrete can be explained by the difference in the damage developing trend under different strain rates.

The mechanism for the size effect is largely related to the coarse aggregate volume ratio. For a larger sample, the coarse aggregate volume is relatively smaller, so that the crack can easily bypass the coarse aggregates to propagate downward along the weak path in the sample. In this way, the damage evolution will be smoother and more thorough. On the contrary, for a smaller sample, the coarse aggregate volume is relatively larger, so that the crack cannot easily bypass coarse aggregates to propagate forward. Consequently, the damage evolution is insufficient, and the failure mode will form a concentrated pattern. Therefore, the strain rate sensitivity of fly ash concrete is gradually reduced with the decrease of size.

From the perspective of energy, most of the energy input by the testing machine in the initial loading stage is stored in the sample in the form of elastic strain energy. Under a higher strain rate, the plastic deformation energy will exceed the elastic strain energy, and the energy is mostly released in the form of fracture surface energy, frictional heat energy and plastic deformation energy. Therefore, the sample exhibits a ductile failure mode. Under a lower strain rate, the elastic strain energy of the sample is higher than the plastic deformation energy, leading to a brittle failure mode.

The influence of specimen inertial effects on the test results is further discussed herein. Within the strain rate

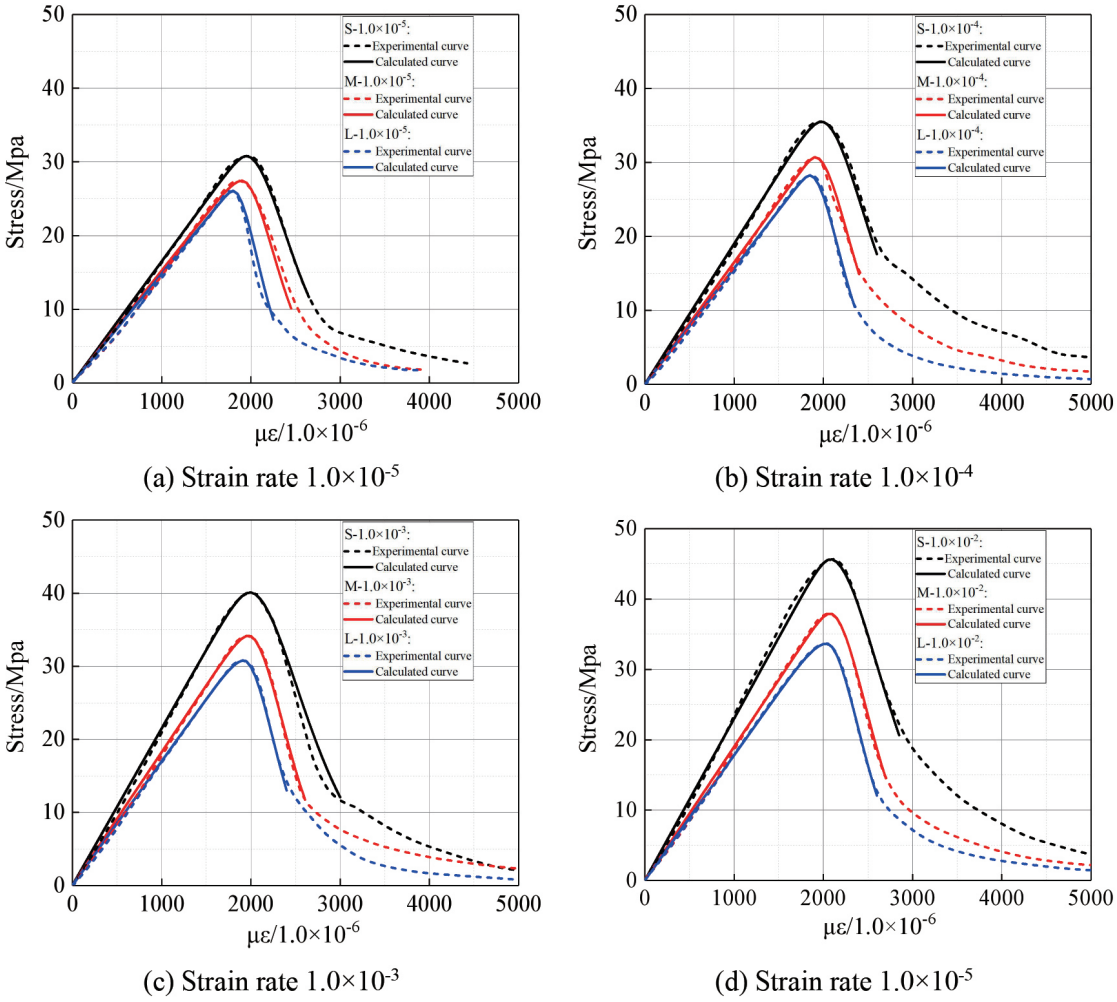


Fig. 21. Comparison between stress-strain curves obtained from experiment and obtained by mathematical regression for fly ash concrete with different sizes under different strain rates.

range of 1.0×10^{-5}-1.0×10^{-2}/s, the dominant strengthening mechanism differs from that under higher strain rate conditions. The intrinsic strain rate effect of the material in this range primarily originates from the time-dependent evolution of microcrack dynamics. A higher loading rate limits stress relaxation at the crack tip, allowing a greater number of microcracks to participate simultaneously in load bearing. This not only manifests as an increase in nominal strength but also alters the energy dissipation path within the specimen. In contrast, the radial inertial effect, as an extrinsic strengthening factor, mainly couples with the inherent confining pressure sensitivity of the compressive strength of concrete. Under higher strain rate impact loading, such as in split Hopkinson pressure bar (SHPB) tests, it makes a significant contribution to the increase in nominal strength.

In summary, the damage evolution of fly ash concrete shows a more uniform distribution pattern under a lower strain rate, and the damage can fully develop throughout the entire concrete structure. The integral damage of the entire sample leads to expansion of micro-cracks to release energy. Under a higher strain rate, the damage evolution is insufficient and mainly takes place around the crack. Consequently, only a few main cracks are formed to release energy. The phenomenon above is ultimately manifested as: the higher the strain rate, the higher the compressive strength is.

4. Conclusions

By considering 3 cylindrical sizes and 4 medium-low strain rates, an experimental study was carried out in this paper to examine the coupling influence of size effect and strain rate effect on the mechanical properties of fly ash concrete based on the developing trend of the stress-strain curve under various working conditions, and the following conclusions were obtained:

(1) The failure mode of fly ash concrete varies greatly under the influence of strain rate effect and size effect. Under the static loading strain rate, the failure mode is manifested as a single, slowly-developing vertical crack on the unloaded surface. As the loading strain rate grows, the failure mode gradually transforms into a rapid-developing damage pattern dominated by multiple oblique small cracks that penetrate the sample. The higher the strain rate, the more serious the damage of aggregates is. Meanwhile, a smaller-sized sample

tends to form more cracks during the failure process. This failure mode is different from that of ordinary concrete.

(2) For the same sample size, the compressive strength, elastic modulus and energy absorption characteristics are all improved gradually as the loading strain rate grows, and their dynamic increase factors have roughly a linear relationship with the dimensionless logarithm of strain rate. For the 3 different sizes "L" , "M" , and "S" , the compressive strength is improved by 29.07%, 38.19% and 48.18%, respectively, under the strain rate effect. Overall, the smaller the size, the higher the strain rate sensitivity is. In addition, the elastic modulus shows a similar developing trend to that of the compressive strength. On the contrary, the energy absorption characteristics of fly ash concrete exhibit a weak strain rate effect but not size effect.

(3) For the same loading strain rate, the compressive strength of fly ash concrete decreases gradually with the increase of size, but the decreasing rate is gradually reduced. When the sample size exceeds the critical dimension, the influence of size effect on the compressive strength can be roughly ignored. Moreover, the critical dimension increases gradually with the increase of strain rate. Under different strain rates, the reduction in compressive strength under the size effect is ranged between 16.89% and 26.26%. Based on the Bazant size effect law, the relationship between the compressive strength and sample size under different strain rates was quantitatively analyzed in this paper.

(4) By referring to the related research conclusions on ordinary concrete, fly ash concrete is more obviously affected by the size effect and strain rate effect compared to ordinary concrete. Based on the Weibull-lognormal statistical distribution, a model describing the stress-strain curve of fly ash concrete under the coupling influence of size effect and strain rate was proposed in this paper, which was verified by comparing with the test data. Finally, the developing trend of the coupling influence of size effect and dynamic rate effect on the mechanical properties of fly ash concrete was comprehensively analyzed to elucidate the underlying mechanisms.

Declaration of Competing Interest

The authors declare that they have no known competing financial interests or personal relationships that could have appeared to influence the work reported in this paper.

CRediT authorship contribution statement

Yaojie Lian: Conceptualization, Data curation, Formal analysis, Writing - original draft, Writing - review & editing.

Data Availability Statement

Some or all data, models, or code that support the findings of this study are available from the corresponding author upon reasonable request.

Acknowledgements

The authors sincerely appreciate the reviewers' insightful and valuable comments and team-mates who make considerable efforts in various way.

References

[1] L.E. Tunstall, G.W. Scherer, R.K. Prud'homme, A new hypothesis for air loss in cement systems containing fly ash, Cement and Concrete Research, 142 (2021).
[2] X. Chen, H. Wang, H. Najm, G. Venkiteela, J. Hencken, Evaluating engineering properties and environmental impact of pervious concrete with fly ash and slag, Journal of Cleaner Production, 237 (2019).
[3] Z. Yu, R. Tang, Z. Guo, Q. Huang, Experimental Study on the Influence of Size Effects on Compressive Dynamic Behavior of Lightweight Concrete, Journal of Materials in Civil Engineering, 34 (2022).
[4] Y. Tan, Y. Cheng, J. Liu, G. Li, Z. Zhang, M. Wang, J. Zhang, Y. Zhang, Experimental Study of the Dynamic Mechanical Properties of High-Performance Equal-Sized–Aggregate Concrete, Journal of Materials in Civil Engineering, 33 (2021).
[5] B.J. Lee, S.-H. Kee, T. Oh, Y.-Y. Kim, Effect of Cylinder Size on the Modulus of Elasticity and Compressive Strength of Concrete from Static and Dynamic Tests, Advances in Materials Science and Engineering, 2015 (2015) 1-12.
[6] P. Chen, C. Liu, Y. Wang, Size effect on peak axial strain and stress-strain behavior of concrete subjected to axial compression, Construction and Building Materials, 188 (2018) 645-655.
[7] L. Jin, W. Yu, X. Du, W. Yang, Dynamic size effect of concrete under tension: A numerical study, International Journal of Impact Engineering, 132 (2019).
[8] J. Fládr, P. Bílý, Specimen size effect on compressive and flexural strength of high-strength fibre-reinforced concrete containing coarse aggregate, Composites Part B: Engineering, 138 (2018) 77-86.
[9] P. Gao, Y. Chen, H. Huang, Z. Qian, E. Schlangen, J. Wei, Q. Yu, Effect of coarse aggregate size on non-uniform stress/strain and drying-induced microcracking in concrete, Composites Part B: Engineering, 216 (2021).
[10] L. Jin, W. Yu, X. Du, W. Yang, Mesoscopic numerical simulation of dynamic size effect on the splitting-tensile strength of concrete, Engineering Fracture Mechanics, 209 (2019) 317-332.
[11] L. Jin, W. Yu, X. Du, S. Zhang, D. Li, Meso-scale modelling of the size effect on dynamic compressive failure of concrete under different strain rates, International Journal of Impact Engineering, 125 (2019) 1-12.
[12] Z.P. Bazant, Size effect in blunt fracture: concrete, rock, metal, J. Eng. Mech., 110 (1984) 518-535.
[13] Z.P. Bazant, Size effect, International Journal of Solids and Structures, 37(1) (2000) 69-80.
[14] W. Weibull, A statistical distribution function of wide Applicability, Appl.Mech.-Trans, 18 (3) (1951) 293–297.
[15] Carpinteri, Fractal nature of material microstructure and size effects on apparent mechanical properties, Mechanics of Materials, 18 (1994) 89-101.
[16] C. Wu, Y. Yang, B. Pang, Y. Cui, The Effect of Different Particle Sizes of Fly Ash on the Properties of Mortar, Materials (Basel), 18 (2025).

[17] W. Zhong, J. Pan, J. Wang, C. Zhang, Size effect in dynamic splitting tensile strength of concrete: Experimental investigation, Construction and Building Materials, 270 (2021).
[18] N.T. Tran, T.K. Tran, D.J. Kim, High rate response of ultra-high-performance fiber-reinforced concretes under direct tension, Cement and Concrete Research, 69 (2015) 72-87.
[19] Y. Hao, H. Hao, G.P. Jiang, Y. Zhou, Experimental confirmation of some factors influencing dynamic concrete compressive strengths in high-speed impact tests, Cement and Concrete Research, 52 (2013) 63-70.
[20] Z. Yu, R. Tang, G. Liu, Z. Guo, Q. Huang, Experimental Study on Dynamic Performance of Plain Concrete and Lightweight Aggregate Concrete under Uniaxial Loading, Journal of Materials in Civil Engineering, 33 (2021).
[21] S. Zhang, R. Song, C. Wang, X. Wang, Experimental Investigation of the Compressive Behavior of RCC under High Strain Rates: Considering the Rolling Technique and Layered Structure, Journal of Materials in Civil Engineering, 30 (2018).
[22] F. Li, G. Chen, H. Long, An Experimental Study Examining the Size Effect on the Compressive Dynamic Performance of Nuclear Power Containment Concrete, Advances in Materials Science and Engineering, 2020 (2020) 1-11.
[23] L. Ma, Z. Li, J. Liu, L. Duan, J. Wu, Mechanical properties of coral concrete subjected to uniaxial dynamic compression, Construction and Building Materials, 199 (2019) 244-255.
[24] Z. Wu, J. Zhang, H. Yu, H. Ma, L. Chen, W. Dong, Y. Huan, Y. Zhang, Coupling effect of strain rate and specimen size on the compressive properties of coral aggregate concrete: A 3D mesoscopic study, Composites Part B: Engineering, 200 (2020).
[25] P.H. Bischoff, S.H. Perry, Compressive behaviour of concrete at high strain rates, Materials and structures, 24(144) (1991) 425-450.
[26] H. Wang, L. Wang, Y. Song, J. Wang, Influence of free water on dynamic behavior of dam concrete under biaxial compression, Construction and Building Materials, 112 (2016) 222-231.
[27] M. Wu, C. Qin, C. Zhang, High Strain Rate Splitting Tensile Tests of Concrete and Numerical Simulation by Mesoscale Particle Elements, Journal of Materials in Civil Engineering, 26 (2014) 71-82.
[28] J. Ozbolt, A. Sharma, H.-W. Reinhardt, Dynamic fracture of concrete – compact tension specimen, International Journal of Solids and Structures, 48 (2011) 1534-1543.
[29] X. Zhang, D. Niu, Dynamic compressive behavior of hybrid basalt-polypropylene fibers reinforced coral aggregate concrete, Journal of Building Engineering, 95 (2024).
[30] H. Nakamura, T. Nanri, T. Miura, S. Roy, Experimental investigation of compressive strength and compressive fracture energy of longitudinally cracked concrete, Cement and Concrete Composites, 93 (2018) 1-18.
[31] J.R. del Viso, J.R. Carmona, G. Ruiz, Shape and size effects on the compressive strength of high-strength concrete, Cement and Concrete Research, 38 (2008) 386-395.
[32] Y. Xu, Y. Chen, Q. Chen, H. Chu, H. Zu, S. Jiang, P. Jiang, M. Juntao, Influence of curing system on static and dynamic mechanical properties of fly ash concrete, Construction and Building Materials, 371 (2023).
[33] C. Lu, Z. Pang, H. Chu, C.K.Y. Leung, Experimental and numerical investigation on the long-term performance of engineered cementitious composites (ECC) with high-volume fly ash and domestic polyvinyl alcohol (PVA) fibers, Journal of Building Engineering, 70 (2023).
[34] K. Ganorkar, M.D. Goel, T. Chakraborty, Specimen Size Effect and Dynamic Increase Factor for Basalt Fiber–Reinforced Concrete Using Split Hopkinson Pressure Bar, Journal of Materials in Civil Engineering, 33 (2021).
[35] Z. Yuan, Y. Jia, X. Xie, J. Xu, Study on the Macroscopic Properties and Microstructure of High Fly Ash Content Alkali-Activated Fly Ash Slag Concrete Cured at Room Temperature, Materials (Basel), 18 (2025).
[36] H. Eker, D. Demir Sahin, M. Çullu, Effect of Reduced Fineness of Fly Ash Used on the Alkali–Silica Reaction (ASR) of Concrete, Iranian Journal of Science and Technology, Transactions of Civil Engineering, 47 (2023) 2203-2217.
[37] L.D. Nhat, V.T. Minh, H. Van Doanh, L.H. Loi, L.Q. Vuong, P.L. Ho, T.T. Thanh, H.D. Tam, Determining the appropriate ratio of fly ash as cement replacement in concrete and evaluating the radiation dose of the fly ash concrete, Journal of Radioanalytical and Nuclear Chemistry, 333 (2024) 5191-5201.
[38] H.-N. Li, P.-F. Liu, C. Li, G. Li, H. Zhang, Experimental research on dynamic mechanical properties of metal tailings porous concrete, Construction and Building Materials, 213 (2019) 20-31.
[39] J. Miltz, G. Gruenbaum, Evaluation of cushioning properties of plastic foams from compressive measurements, Polymer Engineerng & Science, 21(15) (1981) 1010-1014.
[40] P.J. Tan, J.J. Harrigan, S.R. Reid, Inertia effects in uniaxial dynamic compression of a closed cell aluminium alloy foam, Materials Science and Technology, 18 (2013) 480-488.
[41] W. Weibull, A statistical theory of the strength of materials, Ingenoirs Vetenskaps Akadanien Handlinger, 151(15) (1939) 1-45.